



Automated design of a new integrated intelligent computing paradigm for constructing a constitutive model applicable to predicting rock fractures

Kang Peng^{1,2} · Menad Nait Amar³ · Hocine Ouaer⁴ · Mohammad Reza Motahari⁵ · Mahdi Hasanipanah⁶

Received: 8 August 2020 / Accepted: 5 September 2020 / Published online: 18 September 2020
© Springer-Verlag London Ltd., part of Springer Nature 2020

Abstract

Making a relation between strains and stresses is an important subject in the rock engineering field. Shear behaviors of rock fractures have been extensively investigated by different researchers. Literature mostly consists of constitutive models in the form of empirical functions that represent experimental data using mathematical regression techniques. As an alternative, this study aims to present a new integrated intelligent computing paradigm to form a constitutive model applicable to rock fractures. To this end, an RBFNN-GWO model is presented, which integrates the radial basis function neural network (RBFNN) with grey wolf optimization (GWO). In the proposed model, the hyperparameters and weights of RBFNN were tuned using the GWO algorithm. The efficiency of the designed RBFNN-GWO was examined comparing it with the RBFNN-GA model (a combination of RBFNN and the Genetic Algorithm). The proposed models were trained based on the results of a systematic set of 84 direct shear tests gathered from the literature. The finding of the current study demonstrated the efficiency of both the RBFNN-GA and RBFNN-GWO models in predicting the dilation angle, peak shear displacement, and stress as the rock fracture properties. Among the two models proposed in this study, the statistical results revealed the superiority of RBFNN-GWO over RBFNN-GA in terms of prediction accuracy.

Keywords Rock fracture · Radial basis function neural network · Grey wolf optimization · Genetic algorithm

1 Introduction

Rock mass normally comprises rock material and rock discontinuities, and this is characterized by discontinuum constitutive models [1]. On the other hand, making a relation between strains and stresses is an important subject in the rock engineering field. Therefore, this study attempts to present the constitutive models for predicting rock fractures. Literature is consisted of lots of studies carried out into this subject (e.g., Azinfar et al. [2]; Ma et al. [3]; Wang and Tian [4]). Though, according to Jing and Stephansson [5], only two approaches exist to modeling the rock fracture behaviors: (1) the empirical approach, and (2) theoretical approach.

The empirical approach tends to develop the models in the shape of empirical functions that can best represent the experimental data through the use of mathematical regression techniques. This approach does not contain any restraint for respecting the thermodynamics second law. This is worth mentioning that in cases where the parameter ranges and loading conditions are taken into consideration in a proper

✉ Mahdi Hasanipanah
Hasanipanahmahdi@duytan.edu.vn;
Hasanipanah.m@gmail.com

¹ School of Resources and Safety Engineering, Central South University, Changsha 410083, China

² State Key Laboratory of Coal Mine Disaster Dynamics and Control, College of Resources and Safety Engineering, Chongqing University, Chongqing 400044, China

³ Département Études Thermodynamiques, Division Laboratoires, Sonatrach, Boumerdes, Algeria

⁴ Laboratoire Génie Physique des Hydrocarbures, Faculté des Hydrocarbures et de la Chimie, Université M'Hamed Bougara de Boumerdes, Avenue de l'Indépendance, 35000 Boumerdes, Algeria

⁵ Department of Civil Engineering, Faculty of Engineering, Arak University, Arak, Iran

⁶ Institute of Research and Development, Duy Tan University, Da Nang 550000, Vietnam

way, these models will be capable of delivering desirable outputs [1]. On the other hand, the theoretical approach consists of thermodynamic considerations; this feature makes assure that the model obeys completely the second law. Though, parameters of the models constructed based on this approach might possess unclear physical meanings or it can be difficult to define the parameters through experiment [5]. Many constitutive models proposed in the literature for rock fractures encompass the key aspects of shear behaviors of rock mass. As a result, there is a need to improve the conventional regression methods and making them more powerful modeling techniques to better capture the nonlinearity of constitutive responses. The tremendous capacity of modern computers together with the high intricacy of shear behaviors of rock joints has made it completely sensible to apply the computational intelligence to the constitutive models formation process. Singh et al. [6] predicted the strength parameters, including uniaxial compressive and shear strength, using artificial neural network (ANN). According to their results, ANN was an acceptable and reliable method in predicting uniaxial compressive and shear strength. Babanouri and Fattahi [1] employed support vector regression (SVM) to present a constitutive model for predicting rock fractures. They indicated the effectiveness of SVM in this field. A new shear strength criterion was presented by Babanouri and Fattahi [7] using a hybrid of teaching–learning-based optimization (TLBO) and neuro fuzzy system. They showed that their proposed model was capable of predicting rock joint shear strength. In another study, Wu et al. [8] offered ANN model to predict peak shear strength for discontinuities, and compared the ANN performance with multivariate regression method. They confirmed the superiority of ANN over regression method in this filed. Furthermore, the use of artificial intelligence methods has been confirmed in some engineering fields [9–40], which demonstrates the effectiveness of these methods for predicting aims.

Radial basis function neural network (RBFNN), as one of the most widespread types of ANNs, has been widely employed in several fields of civil and mining engineering [41–43]. Although, the literature lacks studies attempting

to model the shear behaviors of rock fractures by means of RBFNN. The main contribution of this study is to combine the Genetic Algorithm (GA) and Grey Wolf Optimization (GWO) with the RBFNN model to develop constitutive models for predicting rock fractures.

The rest of this study is organized as follows. In Sect. 2, we mention the research significance. Then, more details regarding the used datasets are stated in Sect. 3. After that, Sects. 4 and 5 explain the implementation of proposed models to predicting rock fractures. Finally, in the sixth and last section, the results of this study and conclusions are provided.

2 Research significance

Determining and predicting the rock fractures is one of the most important issues in rock engineering field. To this end, this study proposes two integrated intelligent computing paradigms for predicting rock fractures. In the proposed models, two optimization algorithms, i.e., GWO and GA are used to improve the performance of RBFNN. To the best of our knowledge, this is the first study that uses the RBFNN-GA and RBFNN-GWO models in the field of rock fractures.

3 Dataset source

The proposed RBFNN-GA and RBFNN-GWO constitutive models were developed based on an experimental database presented in an open source [1]. In this regard, 84 direct shear tests were carried out upon the concrete and plaster replicas of natural rock fractures under various levels of normal stress. The values of joint roughness coefficient (*JRC*), joint wall compressive strength (*JCS*), Young’s modulus (*E*), normal stress (σ_n), basic friction angle (ϕ_b), dilation angle (*d*), peak shear displacement (δ_{peak}) and peak shear stress (τ_p) were measured for all tests. More details regarding the collection of datasets can be found in Babanouri and Fattahi [1]. Table 1 shows the descriptive statistics related to used

Table 1 Descriptive statistics for the used datasets

Descriptive statistics	Parameters							
	<i>JRC</i>	σ_n (MPa)	<i>JCS</i> (MPa)	<i>E</i> (GPa)	ϕ_b (°)	τ_p (MPa)	δ_{peak} (mm)	<i>d</i> (°)
Standard error	0.607	0.073	1.807	0.356	0.323	0.055	0.018	0.449
Median	12.4	1.3	37.37	7.54	28	1.08	0.56	4.9
Standard deviation	5.567	0.670	16.562	3.270	2.962	0.506	0.170	4.115
Kurtosis	– 1.391	– 1.310	– 1.592	– 1.483	– 1.889	– 0.262	0.252	– 0.038
Skewness	0.229	0.035	– 0.209	– 0.014	0.395	0.511	0.729	0.638
Minimum	4.1	0.57	8	2.88	28	0.37	0.29	0
Maximum	18.9	2.5	52.505	11.91	34	2.54	1.11	18.2

datasets. Furthermore, a part of datasets used in this study is given in Table 2. To train the RBFNN-GA and RBFNN-GWO models, JRC , JCS , E , σ_n and ϕ_b were used as input parameters, whereas d , δ_{peak} and τ_p were used as output parameters. About 80% of the gathered data were employed for constructing the models, while the remaining 20% were used for testing the constructed models.

4 Models

The present study proposes two optimized RBFNN models for predicting rock fractures using GWO and GA algorithms. In this section, the background of proposed models are briefly explained. In the first subsection, the background of RBFNN is mentioned, and then in the second subsection, the GWO and GA algorithms are briefly explained.

4.1 Radial basis function neural network

A literature survey reveals that radial basis function neural network (RBFNN) is one of the most widespread types of ANNs [44, 45]. ANNs represent a computational intelligence method that can be used for prediction, patterns recognition, and modeling inputs-outputs relationships without putting on any assumption. They are designed based on nervous system of the human brain. The ANN system is constructed of neurons with the aim of processing the information.

Recently, RBFNN has been largely used in several research areas due to its capacity in obtaining adequate

results [46–48]. A typical RBFNN model consists of three kinds of layers: input, hidden, and output layers. The input data enter from the input layer. Thereafter, this information is directly transmitted to the hidden layer. This latter represents the principal part of RBFNN; it comprises nodes (n_h) and biases (b_h). Moreover, each (n_h) has a specific radial basis function (RBF) that can be figured with two parameters, the center and the width.

During RBFNN training, a transfer of information from input layer to hidden layer is carried out, where the main goal is to obtain a nonlinear form. Among RBF types, the Gaussian function is mostly used. This function is described by its center (c_i) and spread coefficient (σ^2). The position of input vector (x) according to the center (c_i) is calculated using the Euclidian norm:

$$z_i = \sqrt{\sum_{k=1}^d (x_k - c_{ki})^2} \tag{1}$$

where d and c_{ki} indicate the number of variables and the centers, respectively. After that, the obtained distance is introduced into the Gaussian function, and the following formulation is acquired:

$$\Phi(z) = \exp\left[-\frac{z^2}{2\sigma^2}\right] \tag{2}$$

where the parameters Φ , z and σ^2 denote the Gaussian equation, the Euclidian distance, and the spread coefficient, respectively.

The output layer operates linearly on the basis of the following formula:

Table 2 A part of datasets applied to modeling process in this study

Input parameters					Output parameters			
<i>JRC</i>	σ_n	<i>JCS</i>	<i>E</i>	ϕ_b	τ_p	δ_{peak}	<i>d</i>	
12.4	2.5	17.5	5.32	28	1.42	0.4	4.3	
18.9	2.5	17.5	5.32	28	1.69	0.4	4.3	
4.1	2	17.2	3.86	34	1.61	0.6	0	
18.9	0.57	41.6	8.66	34	0.62	0.58	13.1	
12.4	1.3	52.1	11.36	34	1.12	0.46	9.9	
7.1	0.57	17.2	3.86	34	0.57	0.87	3.9	
12.4	2	37.4	7.54	28	1.08	0.52	6	
18.9	2	17.5	5.32	28	1.67	0.37	8.5	
7.1	1.3	52.5	11.91	28	1.07	0.5	3.4	
18.9	2	52.5	11.91	28	1.67	0.35	11.3	
18.9	2	52.12	11.36	34	2.06	0.5	9.6	
4.1	1.3	52.1	11.36	34	0.64	0.55	3.1	
12.4	0.57	8.0	2.88	28	0.46	0.87	5.6	
18.9	1.3	17.2	3.86	34	1.32	0.8	9.2	
4.1	0.57	52.1	11.36	34	0.39	0.52	3.9	

$$y_j = \sum_{i=1}^{n_h} w_{ij} \Phi_i(z) + b_i, \quad i = 1, \dots, n_h \quad \text{and} \quad j = 1, \dots, N \tag{3}$$

where n_h and N signify the neurons number in the hidden layer and the training samples size, respectively, y_j denotes the j th output of input vector x , w_{ij} is the weight connecting the hidden node i to the output layer, and b_i is the bias.

The performance of RBFNN is completely related to the spread coefficient and the number of neurons in the hidden layer. Thus, the optimum values of these two parameters should be determined using different metaheuristic algorithms. In the current work, GA and GWO are used for the optimization aim.

4.2 Optimization techniques

4.2.1 Genetic algorithm

Genetic algorithm (GA) is a robust optimization approach first proposed by Holland [49] and Goldberg and Holland [50]. This algorithm was designed to solve different complex optimization problems. It utilizes the principles of natural genetics and natural selection as key operators when dealing with optimizing problems. At the first step of GA, a population of individuals that represent the probable solutions is generated randomly. Different individuals are pointed out in the form of chromosomes. The initialization step is followed by genetic operators, i.e., crossover, reproduction, and mutation. Through the iterative processing of GA, new individuals are produced to replace inappropriate ones according to a fitness function that specifies the objective function to be optimized. The selection operator determines parents from among existing individuals. Then, crossover operator substitutes randomly information between two individuals. The genetic operators are repeated until a stopping criterion is met.

4.2.2 Grey wolf optimization

Grey wolf optimization (GWO) is one of the robust population-based algorithms, which was presented by Mirjalili et al. [51]. The steps followed by GWO during the optimization process are imitated from the group living style and the real behavior of grey wolves. The wolves in a pack are ranked based on their importance into α , β , δ and ω , which affects the movements to be made around the prey [51]. The quality of the wolves is assessed with respect to a fitness function. Accordingly, the three fittest individuals are denoted as α , β and δ , while the rest is considered as ω .

The algorithm starts by generating an initial population of wolves randomly. The positions of these wolves offer possible solution for to the problem in hand. Then, prior

investigation is made, which involves circling around the prey. The wolves surround the prey “ p ” based on the following equation [51]:

$$X_{t+1} = X_t^p - A.D \tag{4}$$

where $(t + 1)$ and t represent the actual and previous iterations, respectively, X_t^p signifies the position of the prey (which is also the position of the best wolf, i.e., α), and D is defined as shown below:

$$D = |C.X_t^p - X_t| \tag{5}$$

where X_t is the position of the wolf, and A and C are known as random relocation terms, and they are formulated as:

$$A = 2a.r_1 - a \tag{6}$$

$$C = 2r_2 \tag{7}$$

where a is frequently decreased linearly from 2 to 0; r_1 and r_2 are random values in the interval of [0, 1].

The wolves (ω) update their positions according to the gained information by the fittest wolves, i.e., α , β and δ . Therefore, the following equation is applied [51]:

$$X_{t+1} = \frac{X^1 + X^2 + X^3}{3} \tag{8}$$

where X^1, X^2 and X^3 are defined as follow:

$$X^1 = X_t^\alpha - A_1 \cdot |C_1 \cdot X_t^\alpha - X_t| \tag{9}$$

$$X^2 = X_t^\beta - A_2 \cdot |C_2 \cdot X_t^\beta - X_t| \tag{10}$$

$$X^3 = X_t^\delta - A_3 \cdot |C_3 \cdot X_t^\delta - X_t| \tag{11}$$

where X^α, X^β , and X^δ are the positions of α, β , and δ , respectively.

After the movement of the wolves, their new positions are evaluated according to the fitness function. Therefore, the new position of the fittest wolf α is validated only if this latter outperforms the previous one.

5 Model development

Before proceeding to the implementation of the proposed paradigms, the collected database was subjected to a pre-processing that involved: (1) normalization of the database between -1 and 1 , and (2) splitting the data into training and testing sets. The training part covering 80% of the points was used for the models building, while the test

set encompassing the rest of the points was applied as blind data to evaluating the reliability of the models with unseen values.

As underlined in the previous sections, GA and GWO were implemented for the aim of optimizing the control parameters of RBFNN, namely the spread coefficient and the number of neurons in the hidden layers. The procedure of the proposed hybridizations is illustrated in Fig. 1. The obtained models are denoted RBFNN-GA and RBFNN-GWO. It is worth noting that mean square error (MSE) was the considered fitness function for both algorithms. This function is defined as shown below:

$$MSE = \frac{\sum_{i=1}^n (t_i - o_i)^2}{n} \tag{12}$$

where n is the number of training data, t_i and o_i represent the real and the predicted values, respectively.

In addition, to gain reliable results using these two nature-inspired algorithms, their control parameters should be well determined, which was done in this study through adopting a tuning procedure. The resultant parameters for GA and GWO are given in Table 3.

Table 3 Setting parameters of GA and GWO

Algorithm	Parameters	Value/setting
GA	Population size	50
	Crossover's probability	90%
	Mutation's probability	10%
	Type of selection	Linear ranking
	Max number of generation	50
GWO	Number of wolves	50
	Max number of iterations	50
	a	Linearly decreased from 2 to 0

6 Analysis of the results

In this study, RBFNN-GA and RBFNN-GWO models were proposed to predict τ_p , δ_{peak} , and d parameters. Table 4 reports the final RBFNN control parameters obtained after the optimization using GA and GWO for the three outputs, i.e., τ_p , δ_{peak} , and d . This table reveals that the proposed models for the three outputs yielded their reliable results when the number of nodes was set to a value between 49 and

Fig. 1 Workflow of the proposed hybridizations

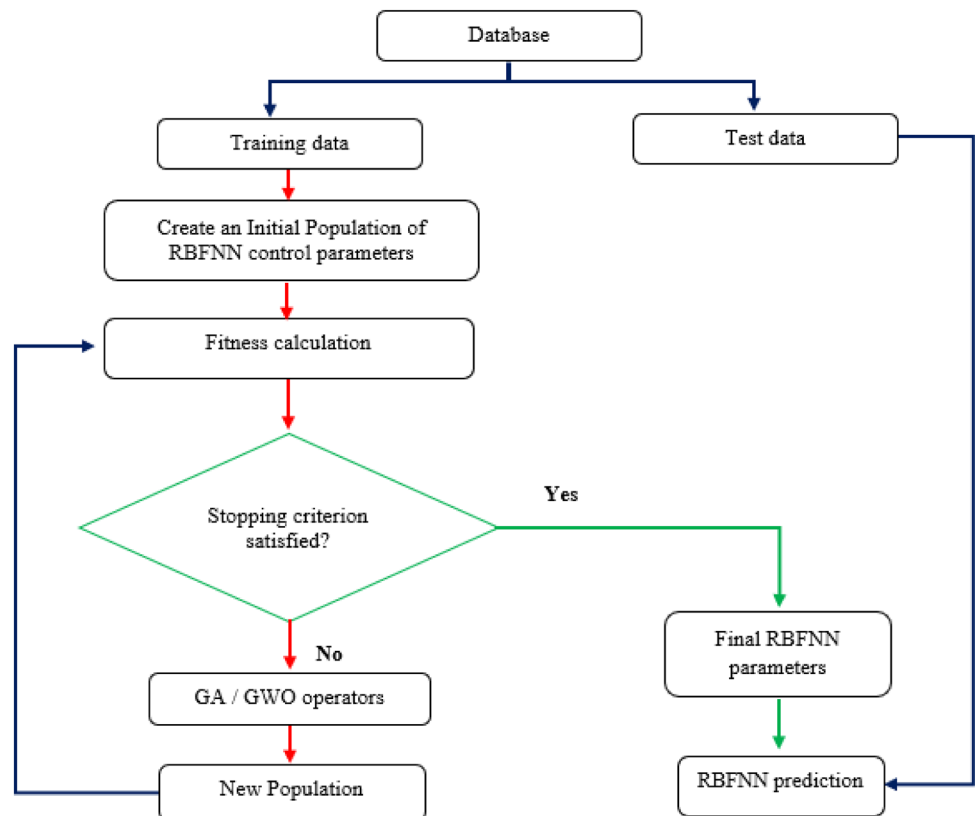


Table 4 Final values of the RBFNN control parameters

Control parameters	RBFNN-GA			RBFNN-GWO		
	τ_p	δ_{peak}	d	τ_p	δ_{peak}	d
Number of nodes	54	53	53	63	49	54
Spread coefficient	1.0698	1.4713	0.9313	0.7589	1.0619	1.0803

Table 5 Statistical functions values obtained from the predictive models

Output	Model	Statistical functions					
		R^2		RMSE		MAE	
		Train	Test	Train	Test	Train	Test
d	RBFNN-GA	0.995	0.921	0.295	1.468	0.231	1.277
	RBFNN-GWO	0.997	0.949	0.212	0.988	0.160	0.850
τ_p	RBFNN-GA	0.999	0.901	0.017	0.223	0.013	0.121
	RBFNN-GWO	1	0.960	0.002	0.095	0.001	0.071
δ_{peak}	RBFNN-GA	0.939	0.904	0.041	0.056	0.030	0.045
	RBFNN-GWO	0.950	0.942	0.037	0.054	0.027	0.044

63; while moderate values for the spread coefficient were noticed in all the models.

To validate and compare the acquired results from the RBFNN-GA and RBFNN-GWO models, three statistical functions, namely root mean square error (RMSE), coefficient of determination (R^2), and mean absolute error (MAE), were used. These statistical functions are expressed by the following formula [52–74]:

$$RMSE = \sqrt{\frac{\sum_{i=1}^n (O_i - P_i)^2}{n}} \tag{13}$$

$$R^2 = \frac{(\sum_{i=1}^n (O_i - \bar{O}_i)(P_i - \bar{P}_i))^2}{\sum_{i=1}^n (O_i - \bar{O}_i)^2 \sum_{i=1}^n (P_i - \bar{P}_i)^2} \tag{14}$$

$$MAE = \frac{1}{n} \sum_{i=1}^n |O_i - P_i| \tag{15}$$

where n is the number of data, and P_i and O_i represent the predicted and observed values of the output parameters, respectively. Note that three output parameters were used in the modeling processes. The values of R^2 , MAE, and RMSE obtained from RBFNN-GA and RBFNN-GWO models for each output parameter were calculated, as given in Table 5. According to this Table, for all output parameters, the performance of RBFNN-GWO was better than RBFNN-GA. This clearly indicates the effectiveness of GWO, as an effective optimization algorithm, in combination with RBFNN. Furthermore, Figs. 2, 3, 4, 5, 6 and 7 show the R^2 values obtained from the RBFNN-GA and RBFNN-GWO models for all output parameters. Based on these figures, the

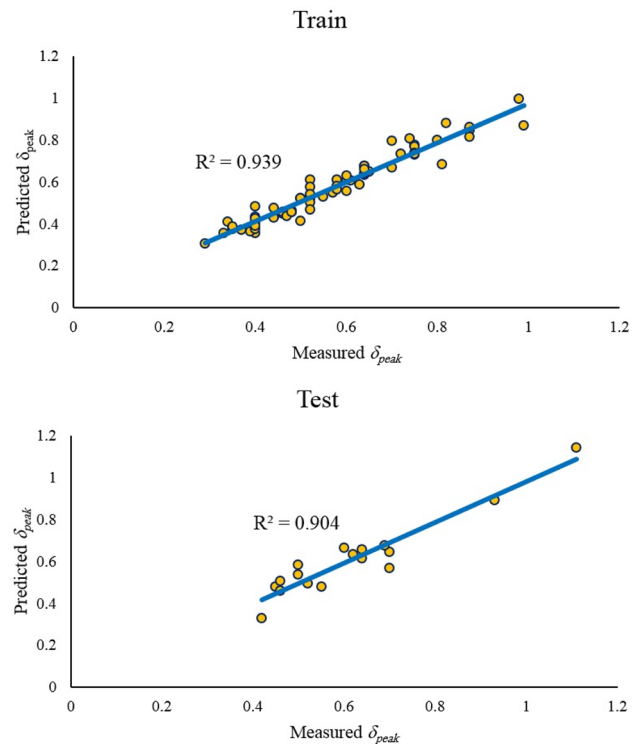


Fig. 2 The measured δ_{peak} vs predicted δ_{peak} using RBFNN-GA

RBFNN-GWO model can be introduced as a robust machine learning model for the prediction of τ_p , δ_{peak} , and d .

For further investigation of the accuracy of the established RBFNN-GWO, Fig. 8 illustrates the relative error distribution between the real values of τ_p , δ_{peak} and d , and predictions of the RBFNN-GWO model. Moreover, Fig. 9 shows the cumulative distribution of the absolute relative

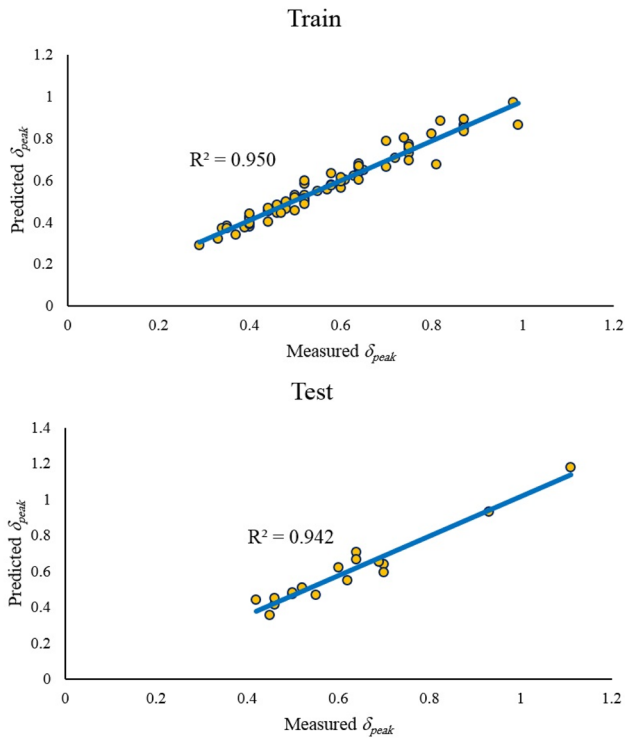


Fig. 3 The measured δ_{peak} vs predicted δ_{peak} using RBFNN-GWO

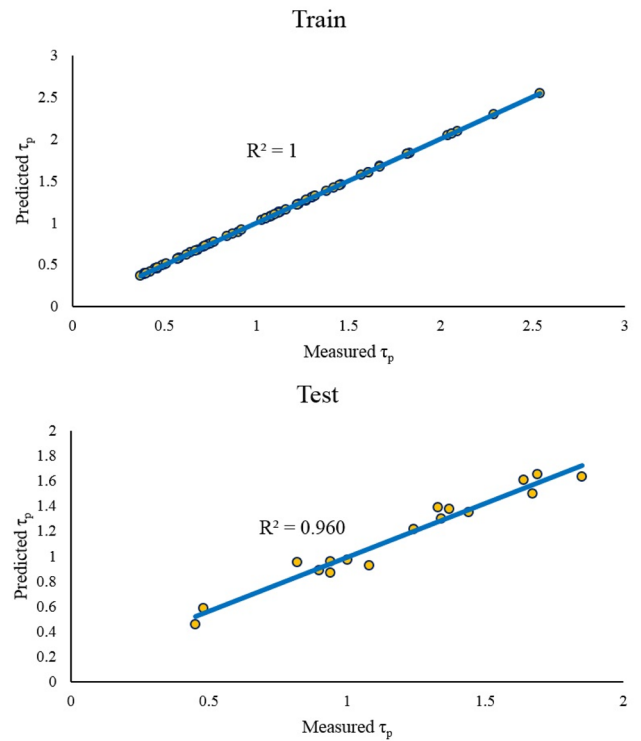


Fig. 5 The measured τ_p vs predicted τ_p using RBFNN-GWO

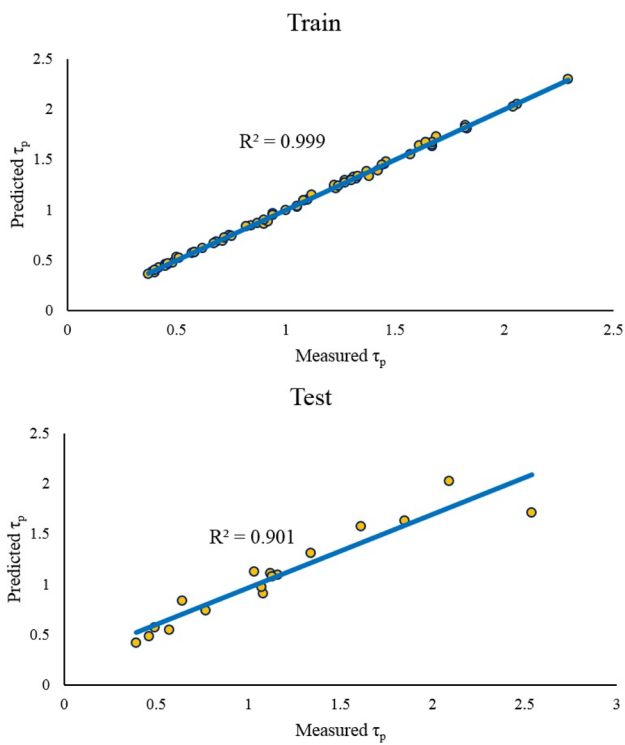


Fig. 4 The measured τ_p vs predicted τ_p using RBFNN-GA

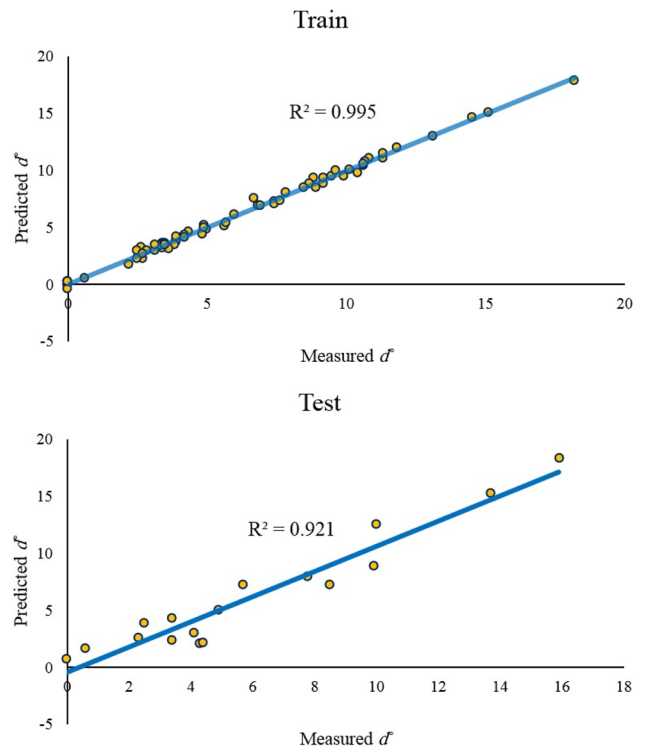


Fig. 6 The measured d vs predicted d using RBFNN-GA

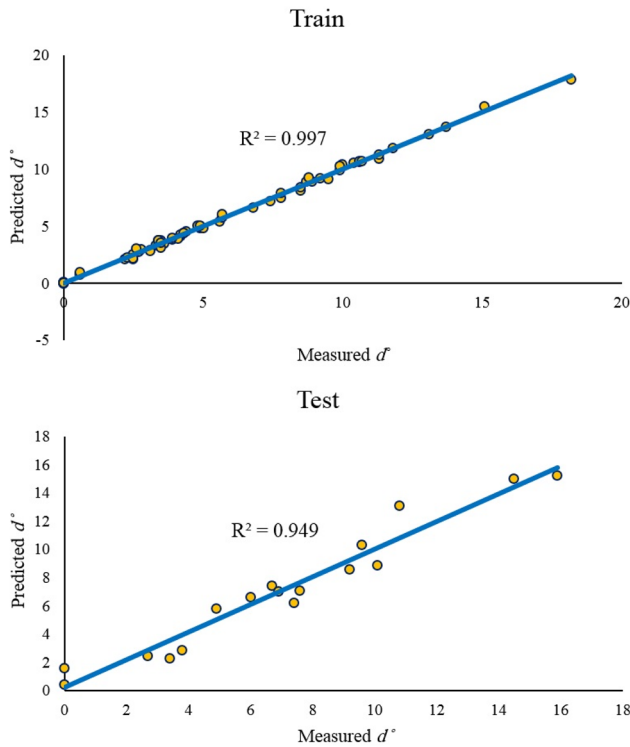


Fig. 7 The measured d vs predicted d using RBFNN-GWO

deviation of the model for the three outputs. It is worth mentioning that in these two figures, some points having zero value of the output, mainly for the case of d , are not exhibited as these points correspond to an infinite value of relative error. However, the points with a zero-value output are well exhibited in the previous cross plots and are mostly located nearby the unit slope line. As it can be seen in Fig. 9, the predictions of RBFNN-GWO follow a satisfactory distribution nearby the zero-error line. In addition, Fig. 9 clearly shows that a great part of the points is predicted by the established RBFNN-GWO with a low AARD. As a matter of fact, 80% of the points are predicted with AARD values of 0.96%, 9%, and 9.66% for τ_p , δ_{peak} and d , respectively. These two figures confirm the reliability of the proposed RBFNN-GWO in predicting the three outputs.

As mentioned earlier, the datasets used in this study were borrowed from Babanouri and Fattahi [1]. They have developed the support vector regression (SVR) model in combination with the biogeography-based optimization (BBO) algorithm for the prediction of τ_p , δ_{peak} and d . They predicted the τ_p with R^2 values of 0.890 and 0.902 in training and testing phases, respectively, while, the RBFNN-GWO proposed in this study predicted the τ_p with R^2 values of 1 and 0.960 in training and testing phases, respectively. These results signify superiority of RBFNN-GWO over SVR-BBO in prediction of τ_p in terms of performance measures. Moreover, Babanouri and

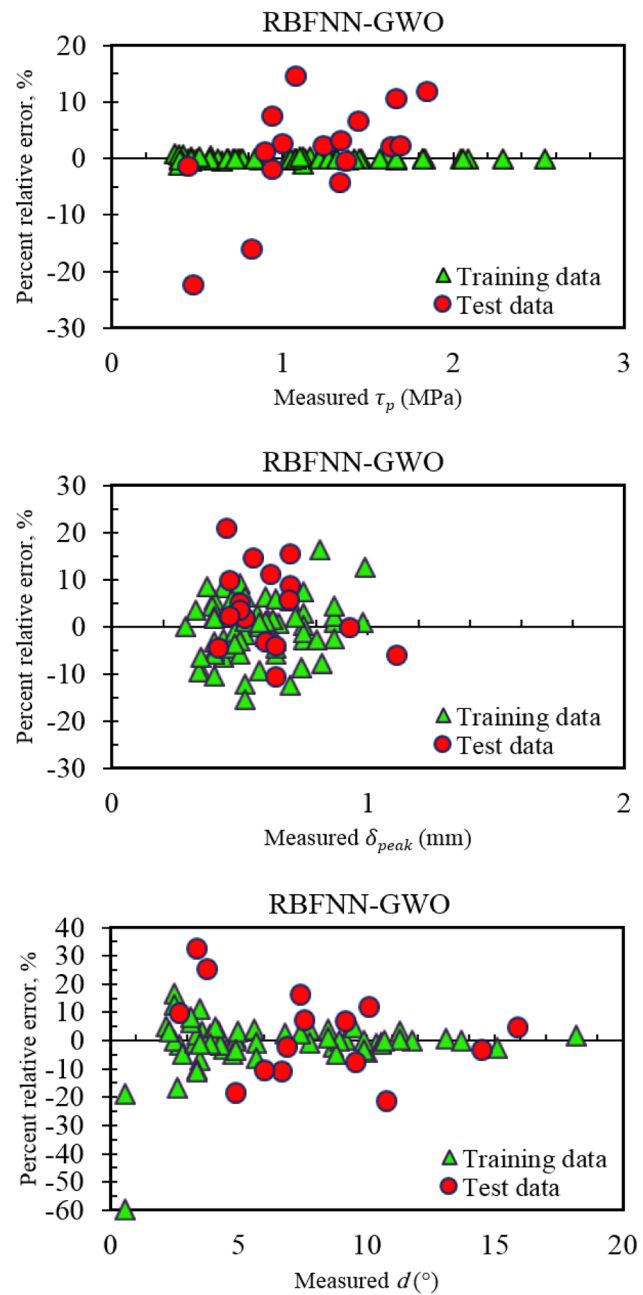


Fig. 8 The relative deviation of the predicted outputs using RBFNN-GWO

Fattahi (2018) predicted the δ_{peak} with R^2 values of 0.949 and 0.888 in training and testing phases, respectively, while the proposed RBFNN-GWO predicted the same parameter with R^2 values of 0.950 and 0.942 in training and testing phases, respectively. Thus, RBFNN-GWO was confirmed superior to SVR-BBO. On the other hand, the d parameter was predicted by Babanouri and Fattahi (2018) using SVR-BBO model with R^2 values of 0.944 and 0.927 in training and testing phases, respectively, while RBFNN-GWO predicted it with R^2 values of 0.997 and 0.949 in

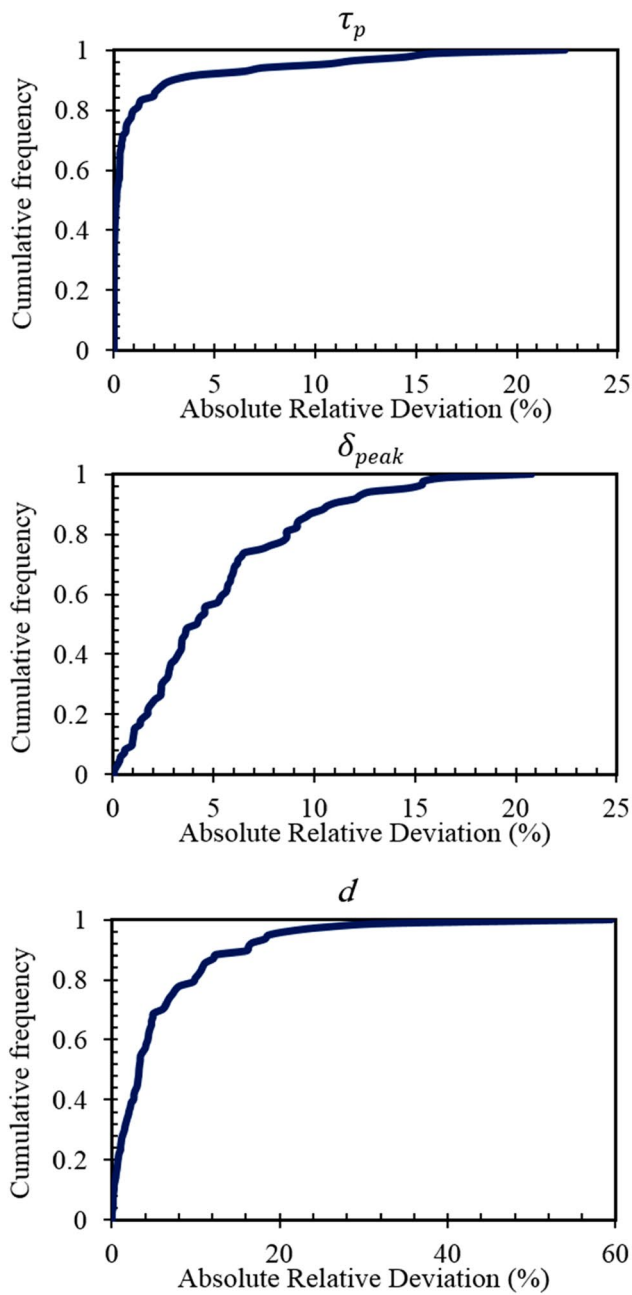


Fig. 9 Cumulative distribution of the absolute relative deviation of RBFNN-GWO

training and testing phases, respectively. These results showed the higher accuracy of RBFNN-GWO than SVR-BBO in predicting d . Accordingly, it can be concluded that RBFNN-GWO outperforms SVR-BBO in terms of prediction capacity. Additionally, the Taylor diagrams related to three output parameters are shown in Fig. 10. Based on this Fig, the RBFNN-GWO model predicted all output parameters with a better accuracy. In the present study, the sensitivity analysis is also performed using Yang and Zang’s [75] method through the following equation:

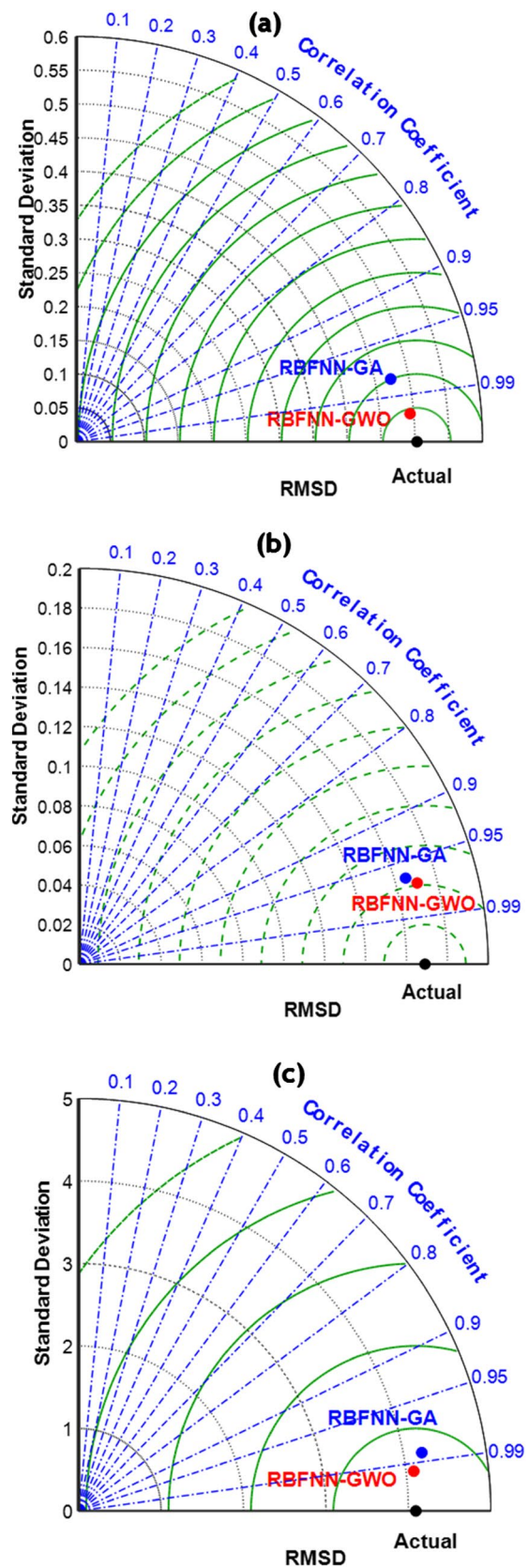


Fig. 10 The obtained Taylor diagrams related to **a** τ_p , **b** δ_{peak} and **c** d

$$r_{ij} = \frac{\sum_{k=1}^n (y_{ik} \times y_{ok})}{\sqrt{\sum_{k=1}^n y_{ik}^2 \sum_{k=1}^n y_{ok}^2}} \quad (16)$$

The values of r_{ij} are varied in range of zero to one, and indicate the impact of each input upon the output. In the modeling, five input parameters, i.e., JRC , JCS , E , σ_n and ϕ_b were used. Also, three parameters, i.e., d , δ_{peak} and τ_p were used as the output parameters. The results of sensitivity analysis are listed below.

- Regarding the first output (d), the values of r_{ij} for input parameters (JRC , JCS , E , σ_n and ϕ_b) were equal to 0.951, 0.794, 0.805, 0.676 and 0.824, respectively. Hence, JRC was the most effective parameter upon d .
- Regarding the second output (δ_{peak}), the values of r_{ij} for input parameters (JRC , JCS , E , σ_n and ϕ_b) were equal to 0.834, 0.817, 0.842, 0.801 and 0.960, respectively. Hence, ϕ_b was the most effective parameter upon δ_{peak} .
- Regarding the third output (τ_p), the values of r_{ij} for input parameters (JRC , JCS , E , σ_n and ϕ_b) were equal to 0.874, 0.839, 0.855, 0.974 and 0.904, respectively. Hence, σ_n was the most effective parameter upon τ_p .

7 Conclusions

Accurate prediction of δ_{peak} , τ_p , and d is an important challenge in the field of rock discontinuities. The present study proposed two hybrid advanced machine learning models, namely RBFNN-GWO and RBFNN-GA, to predict the above-noted parameters. In other words, GWO and GA were used to optimize RBFNN model to see which one works better. To achieve the objective of this study, the required datasets were collected from an open source in the literature (Babanouri and Fattahi 2018). In this regard, the values of JRC , JCS , E , σ_n , ϕ_b , δ_{peak} , τ_p , and d were measured for 84 direct shear tests. In modeling process, JRC , JCS , E , σ_n and ϕ_b were considered as inputs, while δ_{peak} , τ_p , and d were set as outputs. The behaviors of both RBFNN-GWO and RBFNN-GA models were evaluated calculating three statistical functions, i.e., RMSE, R^2 , and MAE.

The conclusions drawn from this study are as follow. (1) While both proposed constitutive models, i.e., RBFNN-GWO and RBFNN-GA, were capable of predicting the δ_{peak} , τ_p , and d , it was found that the RBFNN-GWO prediction performance was more accurate than that of RBFNN-GA. (2) A comparison was made between the performance of RBFNN-GWO presented in this study and SVR-BBO proposed by Babanouri and Fattahi (2018), and according to the obtained results, the performance of RBFNN-GWO model was better than that of SVR-BBO for all output parameters

in both training and testing phases. As an example, the SVR-BBO model predicted τ_p with R^2 values of 0.890 and 0.902 in training and testing phases, respectively, while the values of R^2 obtained from RBFNN-GWO model in training and testing phases were 1 and 0.960, respectively. (3) The RBFNN-GWO model proposed in this study may be applicable to other prediction problems in the rock mechanic fields. (4) It can be also recommended to use other optimization algorithms such as Gradient Evolution Algorithm, Gravitational Search Algorithm, Interior Search Algorithm, Joint Operations Algorithm, Locust Swarm Algorithm, and Sine Cosine Algorithm to optimize RBFNN model.

Acknowledgements This paper is supported by the National Natural Science Foundation of China (51974043, 51774058) and basic scientific research operating expenses of Central Universities (2020CDJQY-A048).

References

1. Babanouri N, Fattahi H (2018) Constitutive modeling of rock fractures by improved support vector regression. *Environ Earth Sci* 77:243
2. Azinfar M, Ghazvinian A, Nejati H (2016) Assessment of scale effect on 3D roughness parameters of fracture surfaces. *Eur J Environ Civ Eng*. <https://doi.org/10.1080/19648.189.2016.1262286>
3. Ma C, Li H, Niu Y (2018) Experimental study on damage failure mechanical characteristics and crack evolution of water-bearing surrounding rock. *Environ Earth Sci* 77:23
4. Wang X, Tian L (2018) Mechanical and crack evolution characteristics of coal–rock under different fracture-hole conditions: a numerical study based on particle flow code. *Environ Earth Sci* 77:297
5. Jing L, Stephansson O (2007) Constitutive models of rock fractures and rock masses—the basics. In: Jing L, Stephansson O (eds) *Fundamentals of discrete element methods for rock engineering theory and applications*. Elsevier, Amsterdam, pp 47–109
6. Singh PK, Tripathy A, Kainthola A, Mahanta B, Singh V, Singh TN (2017) Indirect estimation of compressive and shear strength from simple index tests. *Eng Comput* 33(1):1–11
7. Babanouri N, Fattahi H (2019) An ANFIS–TLBO criterion for shear failure of rock joints. *Soft Comput*. <https://doi.org/10.1007/s00500-019-04230-w>
8. Wu Q, Xu Y, Tang H, Fang K, Jiang Y, Liu C, Wang X (2019) Peak shear strength prediction for discontinuities between two different rock types using a neural network approach. *Bull Eng Geol Environ* 78(4):2315–2329
9. Armaghani DJ, Asteris PG (2020) A comparative study of ANN and ANFIS models for the prediction of cement-based mortar materials compressive strength. *Neural Comput Appl*. <https://doi.org/10.1007/s00521-020-05244-4>
10. Asteris PG et al (2020) A novel heuristic algorithm for the modeling and risk assessment of the COVID-19 pandemic phenomenon. *Comput Model Eng Sci*. <https://doi.org/10.32604/cmescs.2020.013280>
11. Armaghani DJ, Momeni E, Asteris PG (2020) Application of group method of data handling technique in assessing deformation of rock mass. *Metaheuristic Comput Appl* 1(1):1–18. <http://dx.doi.org/10.12989/mca.2020.1.1.001>

12. Asteris PG et al (2020) On the metaheuristic models for the prediction of cement-metakaolin mortars compressive strength. *Metaheuristic Comput Appl* 1(1):63–99. <http://dx.doi.org/10.12989/mca.2020.1.1.063>
13. Apostolopoulou M et al (2020) Mapping and holistic design of natural hydraulic lime mortars. *Cem Concr Res* 136:106167. <https://doi.org/10.1016/j.cemconres.2020.106167>
14. Ly H, Pham BT, Le LM et al (2020) Estimation of axial load-carrying capacity of concrete-filled steel tubes using surrogate models. *Neural Comput Appl*. <https://doi.org/10.1007/s00521-020-05214-w>
15. Apostolopoulou M, Armaghani DJ, Bakolas A, Douvika MG, Moropoulou A, Asteris PG (2019) Compressive strength of natural hydraulic lime mortars using soft computing techniques. *Procedia Struct Integrity* 17:914–923
16. Armaghani DJ, Hatzigeorgiou GD, Karamani Ch, Skentou A, Zoumpoulaki I, Asteris PG (2019) Soft computing-based techniques for concrete beams shear strength. *Procedia Struct Integrity* 17:924–933
17. Asteris PG, Apostolopoulou M, Skentou AD, Antonia Moropoulou A (2019) Application of artificial neural networks for the prediction of the compressive strength of cement-based mortars. *Comput Concr* 24(4):329–345
18. Asteris PG, Armaghani DJ, Hatzigeorgiou Karayannis CG, Pilakoutas K (2019) Predicting the shear strength of reinforced concrete beams using artificial neural networks. *Comput Concr* 24(5):469–488
19. Asteris PG, Ashrafiyan A, Rezaie-Balf M (2019) Prediction of the compressive strength of self-compacting concrete using surrogate models. *Comput Concr* 24(2):137–150
20. Asteris PG, Mokos VG (2019) Concrete compressive strength using artificial neural networks. *Neural Comput Appl*. <https://doi.org/10.1007/s00521-019-04663-2>
21. Asteris PG, Moropoulou A, Skentou AD, Apostolopoulou M, Mohebkhah A, Cavaleri L, Rodrigues H, Varum H (2019) Stochastic vulnerability assessment of masonry structures: concepts, modeling and restoration aspects. *Appl Sci* 9(2):243
22. Asteris PG, Nikoo M (2019) Artificial bee colony-based neural network for the prediction of the fundamental period of infilled frame structures. *Neural Comput Appl* 31(9):4837–4847
23. Cavaleri L, Asteris PG et al (2019) Prediction of surface treatment effects on the tribological performance of tool steels using artificial neural networks. *Appl Sci* 9(14):2788
24. Cavaleri L, Chatzarakis GE, Di Trapani F, Douvika MG, Roinos K, Vaxevanidis NM, Asteris PG (2017) Modeling of surface roughness in electro-discharge machining using artificial neural networks. *Adv Mater Res* 6(2):169–184
25. Chen H, Asteris PG, Armaghani DJ, Gordan B, Pham BT (2019) Assessing dynamic conditions of the retaining wall using two hybrid intelligent models. *Appl Sci* 9:1042
26. Hajihassani M, Abdullah SS, Asteris PG, Armaghani DJ (2019) A Gene expression programming model for predicting tunnel convergence. *Appl Sci* 9:4650
27. Huang L, Asteris PG, Koopialipoor M, Armaghani DJ, Tahir MM (2019) Invasive weed optimization technique-based ANN to the prediction of rock tensile strength. *Appl Sci* 9:5372
28. Psyllaki P, Stamatiou K, Iliadis I, Mourlas A, Asteris PG, Vaxevanidis N (2018) Surface treatment of tool steels against galling failure. *MATEC Web Conf* 188:04024
29. Sarir P, Chen J, Asteris PG, Armaghani DJ, Tahir MM (2019) Developing GEP tree-based, neuro-swarm, and whale optimization models for evaluation of bearing capacity of concrete-filled steel tube columns. *Eng Comput*. <https://doi.org/10.1007/s00366-019-00808-y>
30. Xu H, Zhou J, Asteris PG, Armaghani DJ, Tahir MM (2019) Supervised machine learning techniques to the prediction of tunnel boring machine penetration rate. *Appl Sci* 9(18):3715
31. Hasanipanah M, Zhang W, Armaghani DJ, Rad HN (2020) The potential application of a new intelligent based approach in predicting the tensile strength of rock. *IEEE Access* 8:57148–57157
32. Hasanipanah M, Keshtegar B, Thai DK, Troung NT (2020) An ANN-adaptive dynamical harmony search algorithm to approximate the flyrock resulting from blasting. *Eng Comput*. <https://doi.org/10.1007/s00366-020-01105-9>
33. Hasanipanah M, Bakhshandeh Amnieh H (2020) A fuzzy rule based approach to address uncertainty in risk assessment and prediction of blast-induced flyrock in a quarry. *Nat Resour Res*. <https://doi.org/10.1007/s11053-020-09616-4>
34. Hasanipanah M, Amnieh HB (2020) Developing a new uncertain rule-based fuzzy approach for evaluating the blast-induced back-break. *Eng Comput*. <https://doi.org/10.1007/s00366-019-00919-6>
35. Keshtegar B, Hasanipanah M, Bakhshayeshi I, Sarafraz ME (2019) A novel nonlinear modeling for the prediction of blast induced airblast using a modified conjugate FR method. *Measurement* 131:35–41
36. Sun G, Hasanipanah M, Amnieh HB, Foong LK (2019) Feasibility of indirect measurement of bearing capacity of driven piles based on a computational intelligence technique. *Measurement* 156:107577
37. Nikafshan Rad H, Hasanipanah M, Rezaei M, Eghlim AL (2019) Developing a least squares support vector machine for estimating the blast-induced flyrock. *Eng Comput* 34(4):709–717
38. Luo Z, Hasanipanah M, Amnieh HB, Brindhadevi K, Tahir MM (2019) GA-SVR: a novel hybrid data-driven model to simulate vertical load capacity of driven piles. *Eng Comput*. <https://doi.org/10.1007/s00366-019-00858-2>
39. Lu X, Hasanipanah M, Brindhadevi K et al (2020) ORELM: a novel machine learning approach for prediction of flyrock in mine Blasting. *Nat Resour Res* 29:641–654
40. Ding X, Hasanipanah M, Rad HN, Zhou W (2020) Predicting the blast-induced vibration velocity using a bagged support vector regression optimized with firefly algorithm. *Eng Comput*. <https://doi.org/10.1007/s00366-020-00937-9>
41. Asadzadeh M, Farouq Hossaini M (2016) Predicting rock mass deformation modulus by artificial intelligence approach based on dilatometer tests. *Arab J Geosci* 9:96
42. Wu Q, Shen J, Liu W, Wang Y (2017) A RBFNN-based method for the prediction of the developed height of a water-conductive fractured zone for fully mechanized mining with sublevel caving. *Arab J Geosci* 10:172
43. Rezaei M (2019) Forecasting the stress concentration coefficient around the mined panel using soft computing methodology. *Eng Comput* 35:451–466
44. Tatar A, Naseri S, Bahadori M, Hezave AZ, Kashiwao T, Bahadori A, Darvish H (2016) Prediction of carbon dioxide solubility in ionic liquids using MLP and radial basis function (RBF) neural networks. *J Taiwan Inst Chem Eng* 60:151–164
45. Hemmati-sarapardeh A, Varamesh A, Nait Amar M et al (2020) On the evaluation of thermal conductivity of nanofluids using advanced intelligent models. *Int Commun Heat Mass Transf* 118:104825
46. Haykin S (2001) *Neural networks and learning machines*, 3rd edition, Pearson Upper Saddle River, NJ, USA. [https://doi.org/10.1002/1521-3773\(20010316\)40:6%3c9823::aid-anie9823%3e3.3.co;2-c](https://doi.org/10.1002/1521-3773(20010316)40:6%3c9823::aid-anie9823%3e3.3.co;2-c)
47. Nait Amar M, Jahanbani Ghahfarokhi A, Zeraibi N (2020) Predicting thermal conductivity of carbon dioxide using group of data-driven models. *J Taiwan Inst Chem Eng*. <https://doi.org/10.1016/j.jtice.2020.08.001>

48. Hemmati-Sarapardeh A, Larestani A, Nait Amar M, Hajirezaie S (2020) Applications of artificial intelligence techniques in the petroleum industry. Gulf Professional Publishing. <https://doi.org/10.1016/C2018-0-04421-7>
49. Holland JH (1975) Adaptation in natural and artificial systems. Ann Arbor Univ Michigan Press 1:975
50. Goldberg DE, Holland JH (1988) Genetic algorithms and machine learning. *Mach Learn* 3:95–99
51. Mirjalili S, Mirjalili SM, Lewis A (2014) Grey wolf optimizer. *Adv Eng Softw* 69:46–61
52. Hasanipanah M, Monjezi M, Shahnazar A, Armaghani DJ, Farazmand A (2015) Feasibility of indirect determination of blast induced ground vibration based on support vector machine. *Measurement* 75:289–297
53. Rajabi M, Rahmannedj R, Rezaei M, Ganjalipour K (2017) Evaluation of the maximum horizontal displacement around the power station caverns using artificial neural network. *Tunn Undergr Space Technol* 64:51–60
54. Hasanipanah M, Shahnazar A, Amnieh HB, Armaghani DJ (2017) Prediction of air-overpressure caused by mine blasting using a new hybrid PSO–SVR model. *Eng Comput* 33(1):23–31
55. Hasanipanah M, Armaghani DJ, Amnieh HB, Majid MZA, Tahir MMD (2017) Application of PSO to develop a powerful equation for prediction of flyrock due to blasting. *Neural Comput Appl* 28(1):1043–1050
56. Rezaei M, Hossaini MF, Majidi A, Najmoddini I (2017) Determination of the height of distressed zone above the mined panel: an ANN model. *Int J Min Geo-Eng* 51(1):1–7
57. Qi CC, Fourie A, Chen QS (2018) Neural network and particle swarm optimization for predicting the unconfined compressive strength of cemented paste backfill. *Constr Build Mater* 159:473–478
58. Rezaei M (2018) Indirect measurement of the elastic modulus of intact rocks using the Mamdani fuzzy inference system. *Measurement* 129:319–331
59. Qi CC, Fourie A, Chen QS, Zhang QL (2018) A strength prediction model using artificial intelligence for recycling waste tailings as cemented paste backfill. *J Clean Product* 183:566–578
60. Hasanipanah M, Bakhshandeh Amnieh H, Arab H, Zamzam MS (2018) Feasibility of PSO–ANFIS model to estimate rock fragmentation produced by mine blasting. *Neural Comput Appl* 30(4):1015–1024
61. Qi CC, Fourie A, Chen QS, Tang XL, Zhang QL, Gao RG (2018) Data-driven modelling of the flocculation process on mineral processing tailings treatment. *J Clean Product* 196:505–516
62. Amiri M, Hasanipanah M, Amnieh HB (2019) Predicting ground vibration induced by rock blasting using a novel hybrid of neural network and itemset mining. *Neural Comput Appl*. <https://doi.org/10.1007/s00521-020-04822-w>
63. Asadizadeh M, Rezaei M (2019) Surveying the mechanical response of non-persistent jointed slabs subjected to compressive axial loading utilising GEP approach. *Int J Geotech Eng*. <https://doi.org/10.1080/19386362.2019.1596610>
64. Zhou J, Li C, Arslan CA, Hasanipanah M, Amnieh HB (2019) Performance evaluation of hybrid FFA–ANFIS and GA–ANFIS models to predict particle size distribution of a muck-pile after blasting. *Eng Comput*. <https://doi.org/10.1007/s00366-019-00822-0>
65. Qi CC, Fourie A (2019) Cemented paste backfill for mineral tailings management: review and future perspectives. *Miner Eng* 144:106025
66. Rezaei M, Rajabi M (2019) Assessment of plastic zones surrounding the power station cavern using numerical, fuzzy and statistical models. *Eng Comput*. <https://doi.org/10.1007/s00366-019-00900-3>
67. Yang H, Nikafshan Rad H, Hasanipanah M, Amnieh HB, Nekouie A (2019) Prediction of vibration velocity generated in mine blasting using support vector regression improved by optimization algorithms. *Nat Resour Res*. <https://doi.org/10.1007/s11053-019-09597-z>
68. Benamara C, Nait Amar M, Gharbi K, Hamada B (2019) Modeling wax disappearance temperature using advanced intelligent frameworks. *Energy Fuels* 33:10959–10968
69. Yang H, Hasanipanah M, Tahir MM, Bui DT (2019) Intelligent prediction of blasting-induced ground vibration using ANFIS optimized by GA and PSO. *Nat Resour Res*. <https://doi.org/10.1007/s11053-019-09515-3>
70. Rezaei M, Asadizadeh M (2020) Predicting unconfined compressive strength of intact rock using new hybrid intelligent models. *J Min Environ* 11(1):231–246
71. Qi CC (2020) Big data management in the mining industry. *Int J Miner Metall Mater* 27:131–139
72. Xu C, Nait Amar M, Ghriga MA et al (2020) Evolving support vector regression using Grey Wolf optimization; forecasting the geomechanical properties of rock. *Eng Comput*. <https://doi.org/10.1007/s00366-020-01131-7>
73. Hasanipanah M, Meng D, Keshtegar B et al (2020) Nonlinear models based on enhanced Kriging interpolation for prediction of rock joint shear strength. *Neural Comput Appl*. <https://doi.org/10.1007/s00521-020-05252-4>
74. Ye J, Dalle J, Nezami R et al (2020) Stochastic fractal search-tuned ANFIS model to predict blast-induced air overpressure. *Eng Comput*. <https://doi.org/10.1007/s00366-020-01085-w>
75. Yang Y, Zang O (1997) A hierarchical analysis for rock engineering using artificial neural networks. *Rock Mech Rock Eng* 30:207–222

Publisher's Note Springer Nature remains neutral with regard to jurisdictional claims in published maps and institutional affiliations.